Flash drought early warning based on the trajectory of solar-induced chlorophyll fluorescence

Koushan Mohammadi[a], Yelin Jiang[a], and Guiling Wang[a,1]

Flash drought often leads to devastating effects in multiple sectors and presents a unique challenge for drought early warning due to its sudden onset and rapid intensification. Existing drought monitoring and early warning systems are based on various hydrometeorological variables reaching thresholds of unusually low water content. Here, we propose a flash drought early warning approach based on spaceborne measurements of solar-induced chlorophyll fluorescence (SIF), a proxy of photosynthesis that captures plant response to multiple environmental stressors. Instead of negative SIF anomalies, we focus on the subseasonal trajectory of SIF and consider slower-than-usual increase or faster-than-usual decrease of SIF as an early warning for flash drought onset. To quantify the deviation of SIF trajectory from the climatological norm, we adopt existing formulas for a rapid change index (RCI) and apply the RCI analysis to spatially downscaled 8-d SIF data from GOME-2 during 2007–2018. Using two well-known flash drought events identified by the operational US Drought Monitor (in 2012 and 2017), we show that SIF RCI can produce strong predictive signals of flash drought onset with a lead time of 2 wk to 2 mo and can also predict drought recovery with several weeks of lead time. While SIF RCI shows great early warning potential, its magnitude diminishes after drought onset and therefore cannot reflect the current drought intensity. With its long lead time and direct relevance for agriculture, SIF RCI can support a global early warning system for flash drought and is especially useful over regions with sparse hydrometeorological data.

flash drought | drought early warning | solar-induced chlorophyll fluorescence | vegetation | agriculture

Drought influences all regions of the world, with especially damaging effects on water resources and agriculture. Based on the scope and impact, droughts are often classified as meteorological drought, agricultural drought, and hydrological drought; depending on severity and duration, a meteorological drought may or may not lead to a hydrological or agricultural drought. In the conventional notion, drought results from a gradual accumulation of negative precipitation anomalies leading to prolonged water shortage. In the past decade, the term "flash drought" was coined to describe droughts with a rapid onset and intensification caused by heat, precipitation deficit, or their combination (1–7). Most flash droughts feature a rapid decline of soil moisture and can therefore be classified as agricultural drought. A typical flash drought takes 5–30 d to develop (8). While a flash drought may have a short duration of several weeks to a couple of months, an event that starts as a flash drought may continue to develop into a longer-lasting conventional drought. One such example is the 2012 drought in the United States, which has been the focus of many previous studies. The rapid onset and intensification of flash drought often catch stakeholders (e.g., farmers and rangers) off-guard, leaving no time or resources for planning and adaptation (4–9). The "flashness" presents unique challenges for drought monitoring and early warning.

Multiple approaches have been proposed to detect or identify flash droughts, based on a wide variety of variables reflecting the state of water resources, agriculture, and natural ecosystems, including temperature, precipitation, soil moisture, evapotranspiration (ET), potential ET, vapor pressure deficit (VPD), vegetation index, and gross primary productivity (GPP). For example, Mo and Lettenmaier (1, 2, 10) used different combinations of high temperature, low precipitation, low soil moisture, and high or low ET to identify flash drought, depending on whether an event was induced by heat or by the lack of precipitation. Otkin et al. (3,11) used the evaporative stress index (ESI, defined as the standardized anomalies of the actual to potential ET ratio) (12) as a soil moisture indicator and proposed the Rapid Change Index (RCI) of ESI as a metric of rapid drought intensification, and showed that the ESI RCI could detect flash drought onset 4 wk earlier than the operational United States Drought Monitor (USDM). In their study (3), RCI was defined as the accumulated excess of standardized anomaly of

Significance

Flash drought has become increasingly common and threatens global food security. To help proactively manage and prevent the devastating effects of flash drought, we propose a flash drought early warning approach based on unusually slow increases or unusually fast decreases of a spaceborne proxy for plant photosynthesis, the solar-induced chlorophyll fluorescence (SIF). Relative to the operational US Drought Monitor, the SIF-based approach provides a lead time of 2 wk to 2 mo for flash drought onset and several weeks for drought recovery. It shows great potential to support the development of a global, agriculturally relevant early warning system that will help protect human food security, especially for regions where other drought indices are limited by sparse hydrometeorological data.

weekly ESI changes over a certain threshold, and a negative value of RCI indicated an unusually rapid decrease of soil moisture over multiple weeks. Hobbins et al. (13) proposed the Evaporative Demand Drought Index (EDDI), derived from a physically based estimation of the atmospheric evaporative demand. Both ESI and EDDI can serve as drought early warning relative to drought detection by other indicators such as the operational USDM (14, 15).

Agriculture and grassland ecosystems are among the most vulnerable to flash drought. Vegetation responses captured by satellite data such as the Normalized Difference Vegetation Index (NDVI), the Enhanced Vegetation Index (EVI), and solar-induced chlorophyll fluorescence (SIF) can therefore provide useful large-scale information on flash drought development and impact. NDVI and EVI are more indicative of vegetation greenness, which responds to water stress over a long period and with a delay. However, SIF varies with plant physiological and biochemical conditions and responds rapidly when plants become drought-stressed (16–19), which makes it highly relevant for flash drought monitoring. SIF was found to decline during drought episodes even when NDVI remained constant (20) and showed a clear linear relationship with photosynthesis or GPP at the subseasonal to annual time scales, especially over crop and grass ecosystems (21–27). Sun et al. (28) demonstrated that the satellite-based SIF successfully captured the spatiotemporal pattern of the development and severity of the 2011 drought in Texas and 2012 drought over the Great Plains, showing a strong correlation with soil moisture. Similarly, Chen et al. (29) found that spaceborne SIF successfully characterized the magnitude and spatiotemporal variation of GPP anomalies induced by the 2009–2010 drought in China, and performed better than the greenness-based EVI as a large-scale real-time vegetation drought monitor. Although SIF or anomalies of SIF as used in these studies may perform well as a drought monitor, they cannot provide sufficient lead time to serve as a drought early warning. As global warming causes drought to become more frequent, more intense, or to intensify more rapidly (30–32), drought early warning is becoming increasingly important for regional and global food security. Of particular interest is early warning for droughts that occur at critical stages of crop development including, for example, at the emergence stage or during the early reproductive stage when crops are the most vulnerable to environmental stress (33, 34).

At the early stage of flash drought development, the collective effects of soil moisture depletion, evaporative demand increase, and sometimes heat stress all influence the trajectory of photosynthesis, which may cause slower-than-usual increase or faster-than-usual decrease of GPP and SIF, depending on the timing of drought development relative to the growing season. These trajectory responses precede and ultimately lead to negative SIF anomalies. We therefore hypothesize that an unusual rate of subseasonal change in SIF provides an early warning for flash drought. To test the hypothesis, we quantify the temporal dynamics of SIF prior to and during the 2012 and 2017 flash droughts in the United States using the RCI equations of Otkin et al. (3) (see *Materials and Methods*) and assess the early warning potential of the SIF RCI through comparison with the operational USDM. These two droughts are chosen as case studies because they have been commonly identified as flash droughts, and detailed depiction of drought development is available from the operational USDM (*SI Appendix,* Figs. S1 and S2) and from other studies to facilitate comparison of our results with existing drought metrics (3, 15). While our analyses focus primarily on the downscaled 8-d GOME-2 SIF

data (35–37), we also apply the RCI algorithm to the gap-filled 8-d composite GPP and ET data from MODIS/Terra for comparison, as both are closely related to plant photosynthesis at the process level. In addition, we also examine flash drought development and intensity from a hydrometeorological perspective based on precipitation, temperature, vapor pressure deficit, and short-term drought blend data from GridMET (38).

Results

Flash Drought in 2012. In 2012, abnormal dryness migrated across different regions of the United States, with severe to extreme drought signals over the Great Plains and Midwest starting in July and August; the drought intensified rapidly between July 17 and July 31 over the central United States, expanded in spatial coverage in August, and persisted until the end of the year (*SI Appendix,* Fig. S1). Fig. 1 presents the spatiotemporal patterns of RCI for the 8-d composite SIF during the rapid intensification events in 2012. Prior to the drought in the Midwest and Great Plains region, large positive values of SIF RCI were found in March and early April, reflecting an unseasonal rapid onset of vegetation growth in early spring. However, by May, the SIF RCI transitioned to large negative values. The negative RCI signals reflect an unusually rapid decrease in SIF or, in this case, an unusually slow increase (or even a decrease) at a time when SIF is expected to increase (Fig. 2).

While the trajectory of SIF indicated a deterioration of growth conditions over a large portion of the Great Plains and Midwest starting from early May, the operational USDM did not spot trouble in the region until late June or early July. The SIF RCI signal is the strongest prior to drought onset, and does not (and is not expected to) maintain that strength once drought is in full swing due to the slowing down (or even complete cessation in some areas) of photosynthetic activities leaving little room for SIF to further decrease rapidly. Indeed, as the drought further developed during July–August (*SI Appendix,* Fig. S1), the SIF RCI over most of the drought-stricken regions had small negative values (Fig. 1). However, no persistent spatially coherent positive values of SIF RCI were found through the end of that growing season, indicating that no recovery was yet in sight, consistent with the fact that the drought lasted for over a year.

Interestingly, the strong RCI signal from SIF prior to the 2012 drought was not accompanied by a similar signal from the MODIS GPP or ET data (*SI Appendix,* Figs. S3 and S4). The ET RCI signal was weak overall and spatially scattered. There were negative RCI values for GPP over much of the drought-stricken regions, but they were generally small in magnitude; the strongest signals of negative RCI for GPP were found in late June and July, with a short lead time over the operational USDM. The rather striking magnitude and timing differences between SIF RCI (strongest in May, Fig. 1) and GPP RCI (strongest in July, *SI Appendix,* Fig. S3) may result from differences in sensor sensitivity and ability to capture the fast response of plant photosynthetic activities to environmental stress.

Across most of the United States, the monthly aggregated GPP standardized anomalies were remarkably similar to those of SIF (Fig. 3), which highlights the effectiveness of SIF as an index for vegetation productivity and photosynthetic activities. Both SIF and GPP were unusually high in March and April over much of the eastern United States, but the positive anomalies decreased through the spring and fell below normal by June in most of the Great Plains and Midwest (Fig. 3). The strong positive anomalies of SIF and GPP in March and April (and of ET over the eastern United States) were associated with an
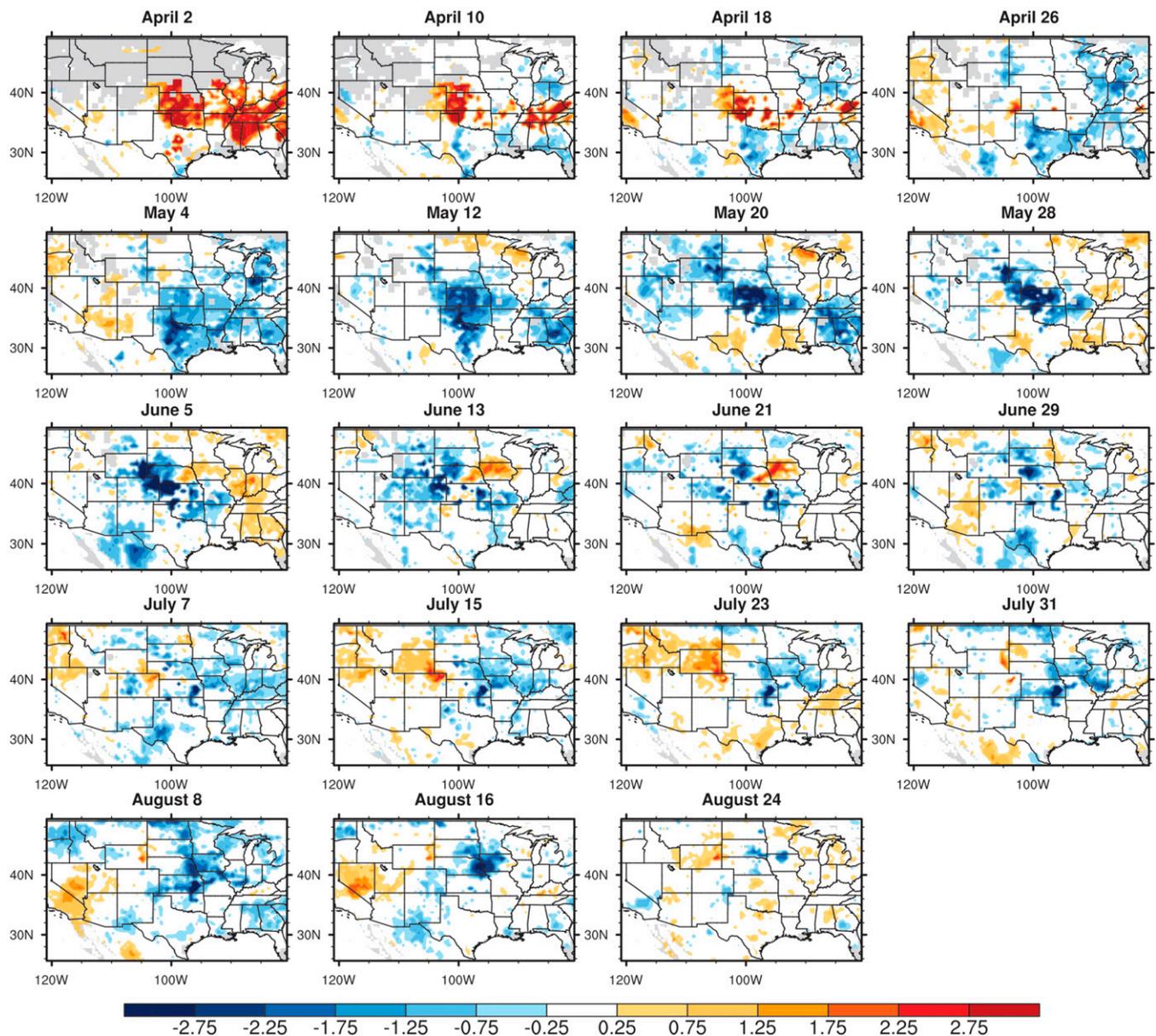
Fig. 1. The 8-d SIF RCI values during April–August 2012. Negative values indicate slower-than-usual increase or faster-than-usual decrease of SIF, while positive values indicate faster-than-usual increase or slower-than-usual decrease of SIF.

abnormally warm condition that kicked off the spring growth way ahead of the normal growing season. This undoubtedly would accelerate soil moisture depletion which, in the absence of strong positive precipitation anomalies, may lead to rapid deterioration of growth conditions for vegetation in late spring/ early summer, reducing GPP and SIF. In fact, precipitation was slightly above normal early in the spring but fell below normal by May. The early onset of growth was not the only factor (and may not even be the primary factor) causing the rapid depletion of soil moisture. The warm condition during spring and summer of 2012 was also accompanied by a persistent higher-than-normal VPD. A recent study (39) found that rapidly developing spring droughts in the central United States typically started with a strong subsidence in the atmosphere, causing an abnormally large VPD prior to the development of other anomalies. The positive VPD anomalies in 2012 likely contributed to the positive ET anomalies in spring (due to high evaporative demand) and the increasingly negative GPP anomalies in spring-summer (by inducing stomata closure in addition to soil

water stress). The first emergence of large negative SIF RCI values at the beginning of May was a result of vegetation integrating the effects of multiple stressors, providing an early warning signal for a potentially rapid drought onset to come. In the several months following, the operational USDM signaled a moderate drought by late June and severe drought by early August (*SI Appendix*, Fig. S1), and the drought severity in some areas underwent a three-category increase over the course of several weeks (3).

Flash Drought in 2017. The 2017 drought was confined to the Northern Great Plains (*SI Appendix*, Fig. S2). The abnormal dryness started over Montana and North Dakota at the end of May, reached the "severe" level in mid-June, and rapidly intensified between July 11th and 25th while also expanding in spatial coverage (toward the northwest and south). The drought reached its peak intensity by August and persisted through September (*SI Appendix*, Fig. S2). The severe drought lasted until October, after which the drought became more moderate but persisted
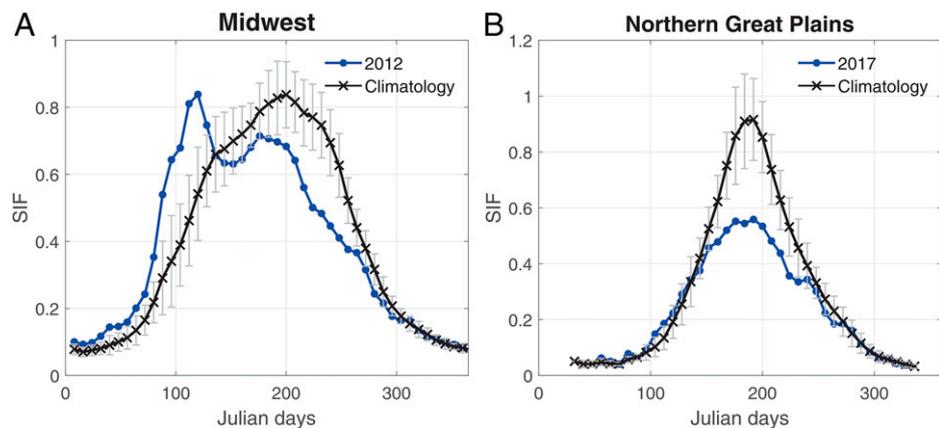
Fig. 2. The 8-d time series of spatially averaged SIF during (*A*) 2012 and (*B*) 2017, in comparison with climatology, for a 5° × 5° sample region in Midwest (35–40°N, 95–100°W) and Northern Great Plains (45–50°N, 100–105°W), respectively.

until the end of the year. The SIF RCI had large negative values from the third week of May through June (Fig. 4), suggesting a rapid deterioration of the vegetation growth condition. Note that a negative RCI value reflects either a faster-than-usual decrease or a slower-than-usual increase; in this particular case, the SIF trajectory showed a much-slower-than-usual increase during May and June, a time frame in which SIF is expected to

rapidly increase in normal years (Fig. 2). The SIF RCI signal disappeared once the drought was in full swing in July, and showed large positive values in August. Clearly, the negative values of SIF RCI preceded the drought onset and the positive values preceded the drought recovery, by 2–4 wk in this case.

The RCI signals of GPP and ET were slightly negative (and scattered) prior to and during the 2017 flash drought over the
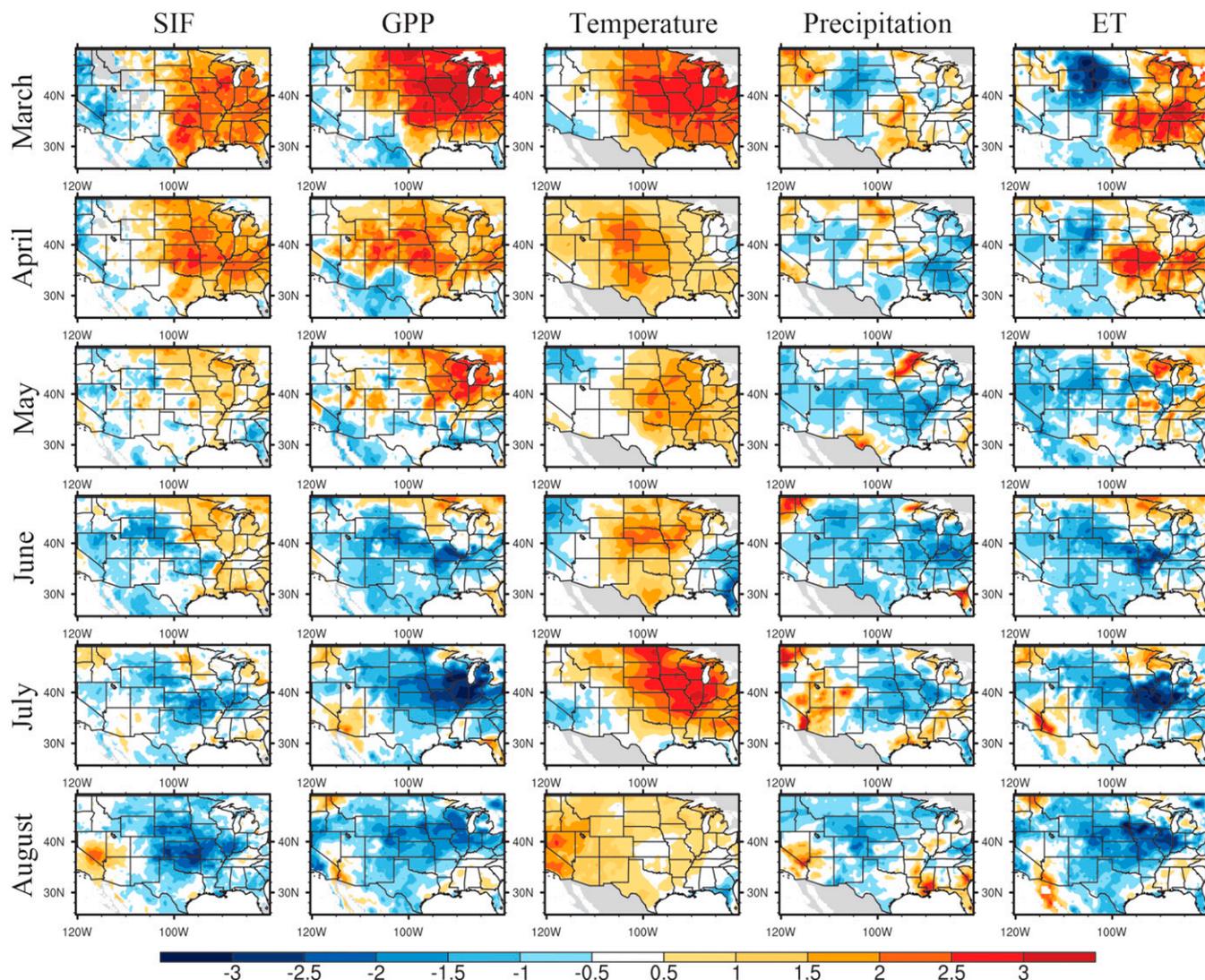
Fig. 3. Standardized anomalies of monthly SIF, GPP, temperature, precipitation, and evapotranspiration prior to and during the 2012 drought.
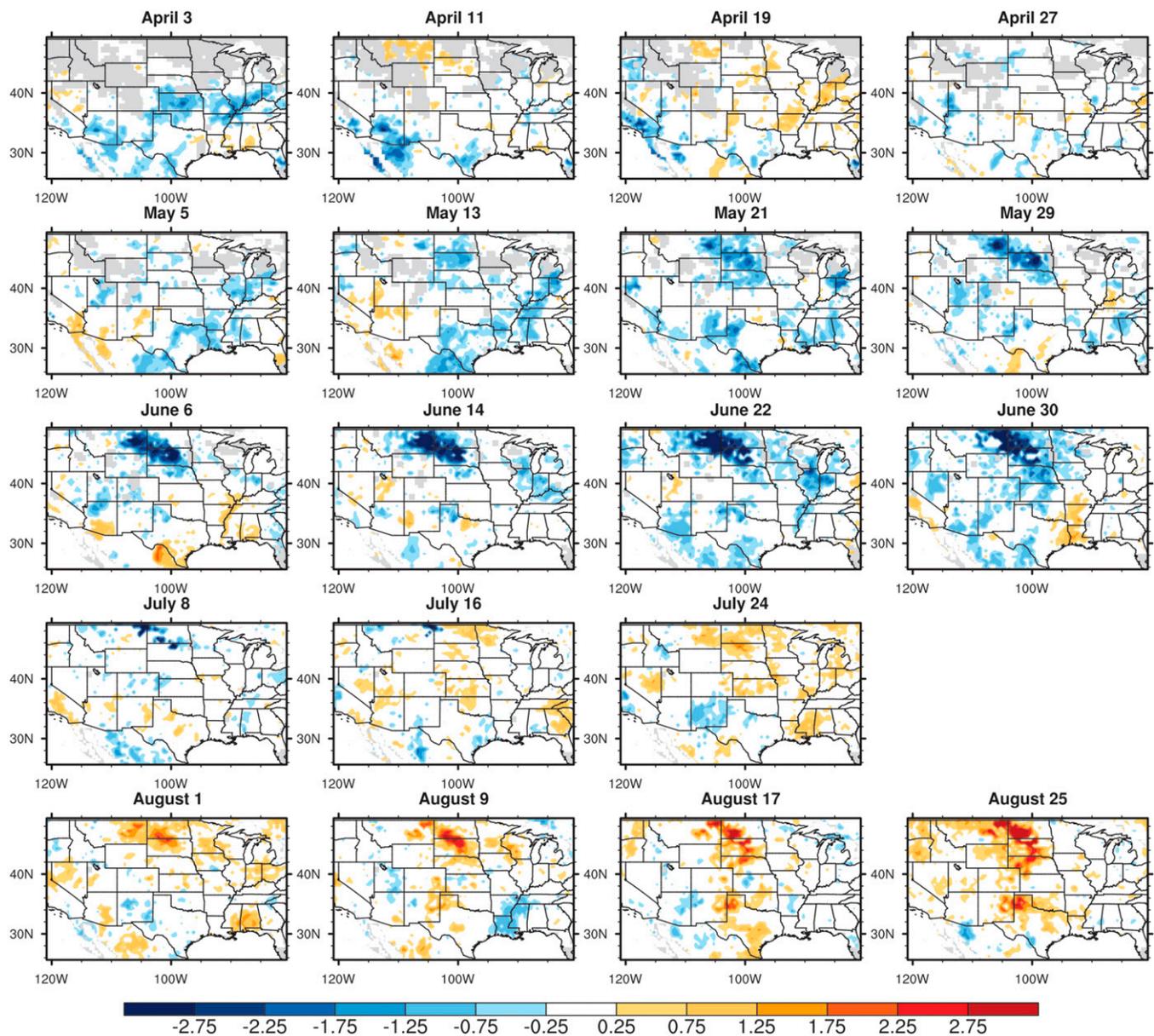
Fig. 4. The 8-d SIF RCI values during April–August 2017. Negative values indicate slower-than-usual increase or faster-than-usual decrease of SIF, while positive values indicate faster-than-usual increase or slower-than-usual decrease of SIF.

drought-stricken region (*SI Appendix*, Figs. S5 and S6) but both showed a strong positive signal in August (similar to the SIF RCI) prior to the drought recovery. Similar to the 2012 event, the SIF temporal dynamics as reflected by RCI showed a much greater sensitivity to environmental condition changes during the early development stage of the 2017 flash drought than other variables analyzed.

During the spring and early summer of 2017, GPP and ET were above normal over most of the United States due to the warm and wet conditions in the spring (Fig. 5), while the corresponding SIF was slightly below normal over most of the United States This discrepancy in the sign of anomalies is a result of the different durations used to define the climatological mean (2007–2018 for SIF, 2001–2019 for GPP and ET), which has little influence on the representation of temporal dynamics and therefore the estimation of RCI under extreme conditions. Indeed, over the northern Great Plains region stricken by the 2017 flash drought, SIF, GPP, and ET were consistent in trajectory and all transitioned from above normal in April to below

normal by June (Fig. 5). The SIF signal experienced the fastest transition among the three, which underlain the strong negative RCI values of SIF in May and June (Fig. 4).

From the meteorological perspective, lower-than-normal precipitation, warmer-than-normal temperature, and higher-than-normal VPD were observed over Montana and North Dakota in the spring and summer. All three contributed to the 2017 flash drought event; none of the individual hydrometeorological variables alone, including temperature, precipitation, VPD, and ET, could provide reliable prediction of the flash drought. The SIF RCI, with the first emergence of large negative values in the middle of May, warned of the 2017 flash drought several weeks earlier than the drought onset indicated by the operational USDM.

Despite compelling evidence for the predictive role of the SIF RCI during the 2012 and 2017 events, limited inventory of flash droughts during the study period precluded a more rigorous assessment on the performance of SIF RCI as a flash drought predictor. As an alternative approach, we challenged the SFI RCI skill against broader benchmarks ranging from wet
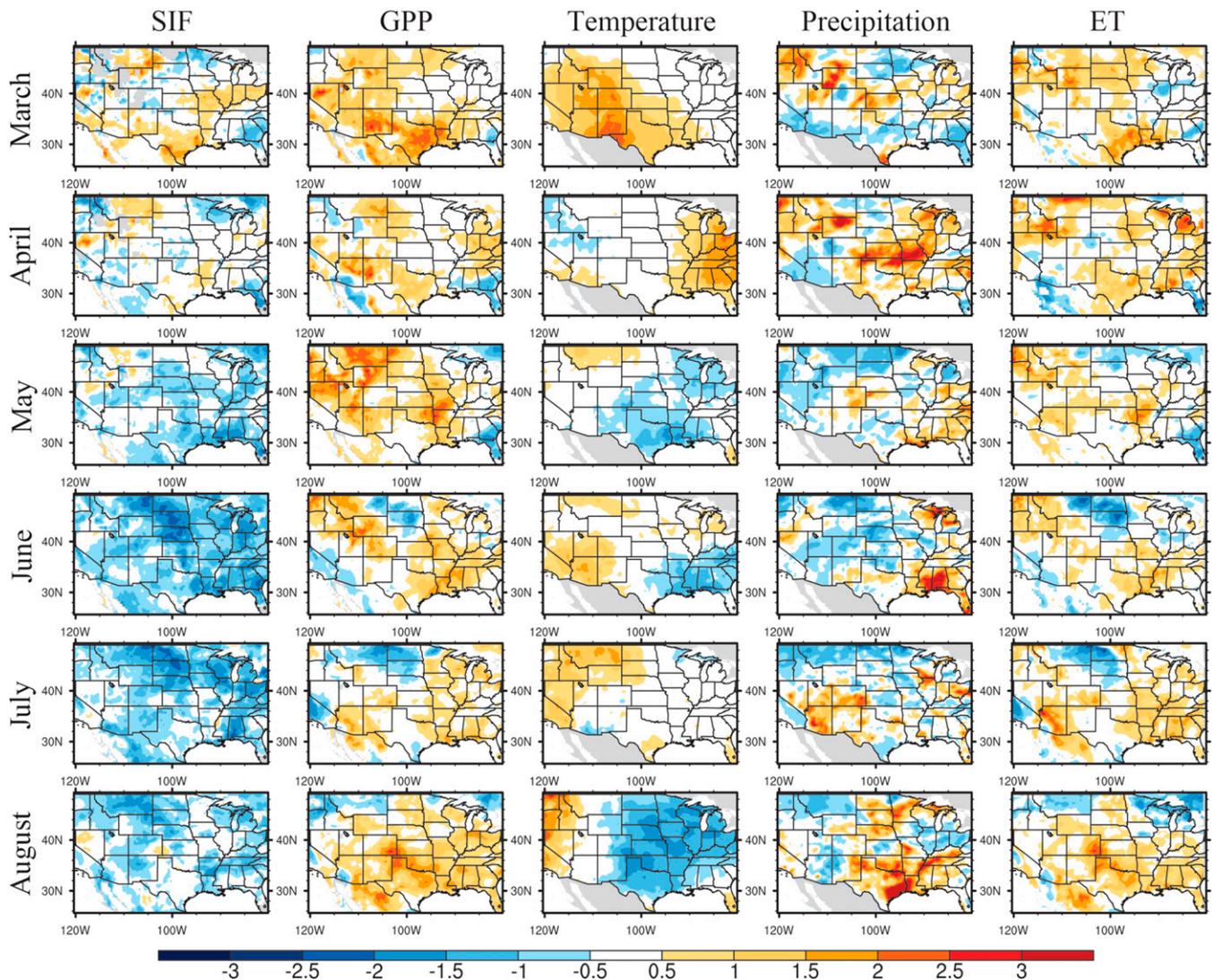
Fig. 5. Standardized anomalies of monthly SIF, GPP, temperature, precipitation, and evapotranspiration prior to and during the 2017 drought.

(favorable) to dry (unfavorable) conditions. Given the overwhelming concern about flash drought impact in the agriculture sector, we examined the predictive relationship of SIF-RCI in May–June with the general water availability and vegetation growth condition in the peak growing season, July–August, in two 5° × 5° sample areas in the Midwest and Northern Great Plains (see *Materials and Methods*). The strongest SIF-RCI signal from May–June was significantly correlated with both the peak ecosystem productivity (reflected by the maximum SIF value) during July–August and the most "relevant" signal of short-term drought blend during July–August (Fig. 6 and *SI Appendix,* Table S1). Judging by the sign of the spatially averaged anomalies, out of the 12 y analyzed, predictions of dry or wet conditions based on SIF RCI would produce no misclassification in the Northern Great Plains sample area and one false alarm in the Midwest sample area (which occurred in a year when both the predictor and the predictand were close to their long-term means) (Fig. 6*B*). Flash droughts are intrinsically extreme and may disproportionately influence the correlation. However, for both sample areas analyzed, excluding the 2012 or 2017 event from the data did not qualitatively change the relationships (Fig. 6 and *SI Appendix,* Table S1). These results provide strong evidence for the robustness of SIF RCI as a predictor for not only flash drought but also general eco-hydrometeorological conditions.

Discussion

This study analyzed satellite-derived data on vegetation functional status prior to and during two major flash droughts in the United States and assessed the potential of sensitive vegetation response as an early warning of flash drought onset. The underlying hypothesis is that slower-than-usual increases or faster-than-usual decreases of plant photosynthetic activities captured by the SIF trajectory at a very early stage of drought development can provide an early warning for flash drought onset. As a quantitative metric, we applied the RCI formulas of Otkin et al. (3) to spaceborne measurements of SIF, GPP, and ET to assess the degree of unusual rates of change, and used the 2012 and 2017 US drought as examples. We found that a large negative RCI value of SIF during the growing season could warn of a flash drought onset at least several weeks before the drought could be detected by the operational USDM. The RCI values of GPP and ET did not provide a reliable or consistent predictor for drought onset. However, a strong positive RCI signal from all three variables (SIF, GPP, and ET) was found to precede drought recovery by several weeks. While our analysis was not exhaustive and was limited by the number of well-documented flash droughts during the time of SIF data availability, our results showed great potential for SIF RCI to be used as a predictor for both flash drought onset and recovery, with several weeks of lead time over
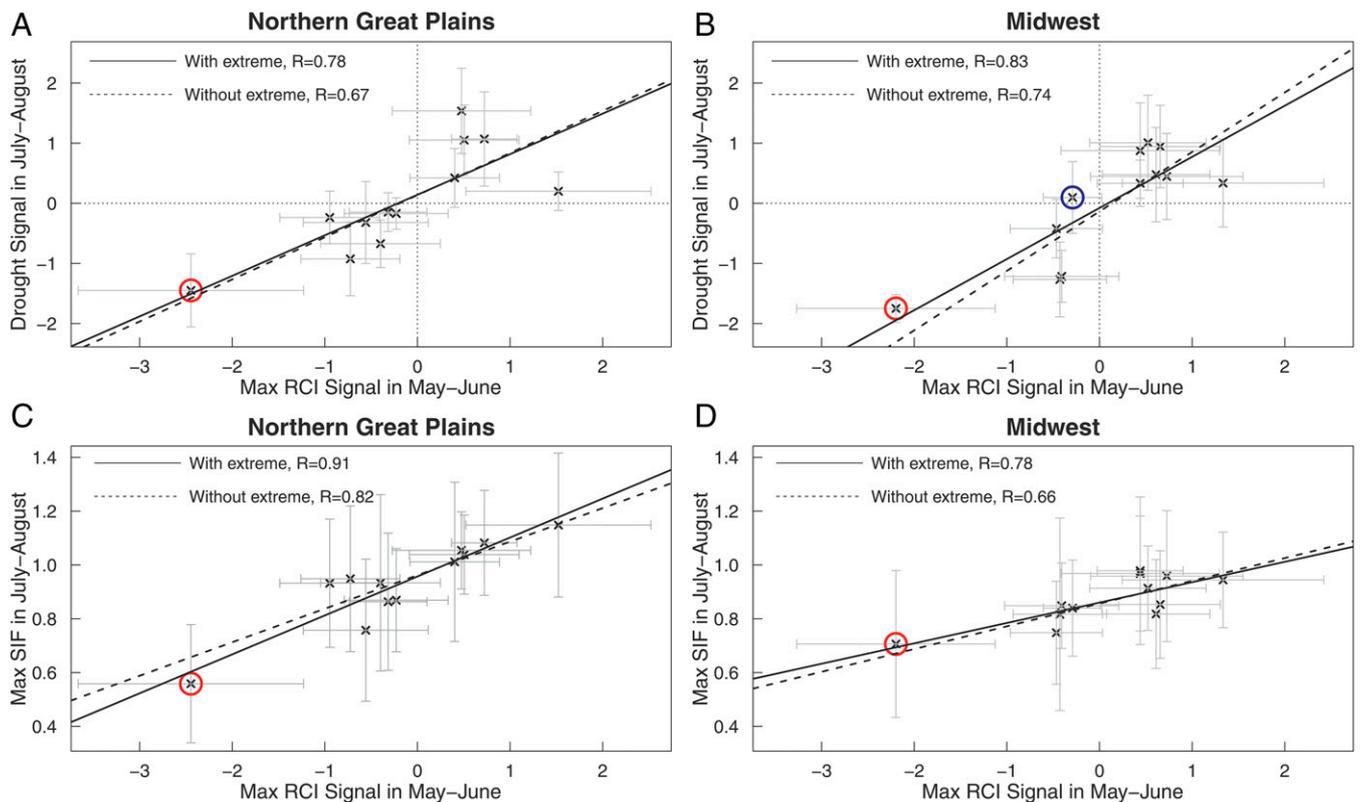
Fig. 6. Scatter plot between the maximum signal of SIF-RCI during May–June and two benchmarks during July–August of 2007-2018: the short-term drought blend (*A* and *B*) and maximum SIF (*C* and *D*), spatially averaged over a 5° × 5° sample region in the Northern Great Plains (45–50°N, 100–105°W) and in the Midwest (35–40°N, 95–100°W) respectively; error bars indicate the spatial variability within the sample area. The maximum RCI signal refers to the RCI value (positive or negative) whose magnitude is the largest among all values during May–June of each year. Also shown are the linear regression lines with (solid) and without (dashed) the extreme drought (marked with a red circle). The blue circle (in *B*) marks the false alarm case for RCI-based drought early warning. All correlations are statistically significant.

the operational USDM. This has significant implications, as the hard-to-predict sudden onset has been a major challenge for coping with the widespread consequences of flash droughts.

In testing the effectiveness of the SIF RCI as a drought early warning index, this study focused on two well-documented events and chose the widely used operational USDM as a reference for comparison. Recently, EDDI (13) has gained wide recognition as a physically based predictive index with a long lead over the operational USDM. It is worth comparing our SIF RCI results with published EDDI results (14, 15). For the 2012 event, the timing of drought signal emergence was similar between SIF RCI and EDDI, both in late April to early May; the SIF RCI signal rapidly intensified in May, reaching the maximum by late May and early June, while the EDDI signal reached the maximum 1 mo later in early July. Another important difference is that after drought onset, EDDI retained its large magnitude reflecting drought intensity, while the magnitude of SIF RCI diminished once the drought was in full swing and could not function as a drought intensity monitor.

The unusual SIF trajectory prior to the flash drought onset is likely a result of vegetation photosynthetic response to multiple stressors at the early stage of drought intensification. The predictive skill of SIF RCI in and of itself does not suggest vegetation to be a causal source of drought predictability. However, in regions of strong land–atmosphere coupling such as the US Great Plains and Midwest (40, 41), vegetation response to drought stress at the subseasonal time scale may feed back to further suppress precipitation and enhance drought severity. For example, numerical modeling experiments showed that dry soil moisture anomalies in late spring/early summer could cause a decrease of summer

precipitation and a major fraction of this effect was attributed to vegetation feedback through a drought-induced decrease of leaf area index (42, 43). This subseasonal vegetation-climate feedback can certainly contribute to the performance of SIF RCI as a drought predictor. More concrete identification of the processes and mechanisms underlying this predictive relationship requires further research beyond the scope of the present study.

The finding that the GPP or ET trajectories are not as effective or sensitive as the SIF trajectory in reflecting drought development warrants further discussion. In the real world, both GPP and ET over vegetated land are closely related to stomatal conductance and plant photosynthesis (therefore SIF). However, from the technical perspective, GPP and ET cannot be directly measured through remote sensing. Instead, they were derived from MODIS using equations that involved remote sensing of photosynthetically active radiation and/or vegetation greenness index as well as meteorological data from reanalysis (44, 45), all of which could be sources of uncertainty. At the process level, although drought-induced stress may cause stomatal closure (which tends to reduce ET and increase canopy temperature), the large vapor pressure deficit (whether dynamically induced due to subsidence or thermally induced by high temperature) increases the atmospheric evaporative demand (which tends to accelerate ET). Due to these competing effects, ET may increase or decrease at the early stage of drought development (46) and therefore cannot serve as a reliable drought predictor.

SIF RCI as an early warning for flash drought has some intrinsic advantages and limitations. Relying on the response of plant photosynthetic activities, SIF RCI is applicable over vegetated land only, and may be more effective in grasslands and

croplands than in forests, due to disparity in SIF's ability to track plant photosynthesis in different ecosystems (17, 25, 47). While this is a limitation, it also makes the index highly relevant for agriculture (including rangelands, pasture, and cropland), the sector most influenced by flash droughts. Herbicides and pests may cause a localized short-lived signal of negative RCI, but such a signal should be easy to distinguish from a flash drought signal (which is typically over a large scale for multiple weeks). The global availability of spaceborne SIF data is a major advantage, especially for regions where the lack of sufficiently accurate meteorological data limits the accuracy of other drought warning tools. The downscaled corrected GOME-2 SIF dataset used, available for the 2007–2018 period, compared remarkably well with SIF data from the Sentinel-5 Precursor Tropospheric Monitoring Instrument (TROPOMI) during their overlapping period, 2018 (36). It can therefore be used as the historical archive for the TROPOMI SIF data to facilitate the derivation of SIF RCI in real time. With its long lead time and direct relevance to agriculture, SIF RCI can support the development of a globally accessible early warning system for flash droughts.

Materials and Methods

In this study, we assessed the temporal dynamics of vegetation functioning prior to and during the 2012 and 2017 US droughts based on data derived from satellite remote sensing. These include the 8-d GOME-2 SIF data downscaled from 0.5° to 0.05° to better capture the spatial heterogeneity of ecosystem activities (35–37), and the gap-filled 8-d composite data from MODIS/Terra on ET (MOD16A2GF) and GPP (MOD17A2HGF) at 500-m spatial resolution (available at https://lpdaacsvc.cr.usgs.gov). The ET and GPP data are available for 2000–2019, and the GOME-2 SIF data are available for 2007–2018. In addition to ET, we also analyzed other hydro-meteorological variables relevant to drought development, including precipitation, temperature, VPD, and short-term drought blend from the GridMET dataset (37), which has a daily time step and 4-km spatial resolution.

Our study used the USDM as the drought metric to characterize the 2012 and 2017 flash droughts. The USDM map shows the weekly updated location and intensity of drought using a five-category system: abnormally dry (D0), moderate drought (D1), severe drought (D2), extreme drought (D3), and exceptional drought (D4). Based on weighted averaging of a large number of indicators (including Palmer Drought Severity Index, soil moisture index, streamflow index, and standardized precipitation index), USDM can account for all types of and all aspects of droughts. Results from our SIF trajectory analyses were compared against USDM to identify the lead time for the SIF-derived drought early warning index.

To quantify how much the temporal change rate of SIF deviated from its climatological mean, we took the RCI formulation of Otkin et al. (3), and applied the RCI approach to the 8-d GOMES-2 SIF data. For comparison with the SIF RCI, we also conducted the RCI analysis for two other satellite-derived variables related to vegetation functioning, the 8-d GPP and ET from MODIS, to assess how different sensors may vary in capturing the temporal dynamics of photosynthesis. For convenience, the following description refers to the 8-d period as a "week."

The RCI estimation involves two steps. First, the standardized anomalies of the temporal change rate of SIF are calculated as:

$$\Delta V(w_1, w_2, y) = \frac{[V(w_2, y) - V(w_1, y)] - \frac{1}{N}\sum_{y=1}^{N}[V(w_2, y) - V(w_1, y)]}{\sigma(w_1, w_2)},$$

where $V(w, y)$ is the SIF composite for week w and year y. On the right-hand side of the equation, the second term in the numerator defines the climatological mean of the rate of change between weeks w_1 and w_2 over N years, and the denominator is its SD for the corresponding time, respectively. A negative ΔV represents a slower-than-usual increase or faster-than-usual decrease of SIF, while a positive ΔV indicates a faster-than-usual increase or slower-than-usual decrease of SIF.

An anomalous weather pattern can persist for multiple weeks and cause drought development or recovery. Therefore, the response of vegetation functioning and moisture stress can be seen through unusual rate of change over an extended period. The second step of the RCI calculation involves the time accumulation of ΔV (3):

$$RCI = RCI_{prev} - \sqrt{abs(\Delta V) - 0.75} \quad if \ \Delta V < -0.75,$$

and

$$RCI = RCI_{prev} + \sqrt{abs(\Delta V) - 0.75} \quad if \ \Delta V > 0.75.$$

Here, RCI_{prev} is the RCI value from the previous week. RCI as formulated above represents the temporal accumulation of excess ΔV above the set threshold of 0.75 (3, 48). The RCI value remains unchanged if ΔV is of the same sign as in the previous week but its magnitude does not exceed the set threshold of 0.75, and is reset to zero if ΔV changes sign from the previous week.

During the growing season, a large negative value of RCI indicates an upcoming drought onset, and a large positive value of RCI indicates an upcoming recovery from drought. RCI is designed to capture temporal dynamics, but does not directly reflect the magnitude or intensity of the drought after its onset. For example, RCI would be close to zero after the onset and before the beginning of the recovery of a long persistent drought. As a monitoring measure for drought intensity (as opposed to early warning), the standardized anomalies of several relevant variables were also analyzed, including SIF, GPP, ET, temperature, precipitation, and VPD. To facilitate comparison, all data at different spatiotemporal resolutions were first aggregated to a common 0.5° and monthly resolution. Standardized anomalies were then estimated as the anomalies (deviation of the monthly data from the climatological mean of that month) divided by the corresponding SD to remove the impact of seasonality.

To examine the robustness of SIF RCI as an early warning index, we expanded our analysis to include the full range of hydro-meteorological conditions. Instead of using the operational USDM data, which focus on dry extremes, we used the short-term blend of drought indicators from gridMET, which ranges from dry to wet. Here we chose the strongest SIF RCI signal (positive or negative) during May–June of each year, and related that to two types of benchmark during the peak growing season, July–August. One was the maximum SIF value as a metric for ecosystem productivity, and one was the short-term drought blend from GridMET as a metric for water availability. The short-term blend in some years showed strong temporal dynamics due to multiple short-duration events. To identify the most "relevant" event in each year, we chose the lowest (highest) short-term blend during July-August if the strongest SIF RCI signal during May–June is negative (positive). We assessed the relationships between the predictor (strongest SIF RCI signal) and the predictands (two benchmarks) over two 5° × 5° sample areas that were hit hard by the 2012 and 2017 flash droughts, respectively, one in Midwest (35–40°N, 95–100°W) and one in Northern Great Plains (45–50°N, 100–105°W).

Since an individual drought event may influence a large area, data from different grid cells within each sample area are not independent. Lumping data from all grid cells in the correlation analysis (e.g., in *SI Appendix*, Fig. S7) would overestimate the degree of freedom (therefore the statistical significance of the correlation). To address this uncertainty, we used the spatial averages of the data across each sample area to derive the least squares linear regression lines and the Pearson correlation coefficients (Fig. 6). The spatial variability within each sample area (as reflected by the error bars around each data point in Fig. 6) is heavily influenced by the size of the sample area and is therefore not intrinsic to the relationships analyzed here.

1. K. C. Mo, D. P. Lettenmaier, Heat wave flash droughts in decline. *Geophys. Res. Lett.* **42**, 2823–2829 (2015).
2. K. C. Mo, D. P. Lettenmaier, Precipitation deficit flash droughts over the United States. *J. Hydrometeorol.* **17**, 1169–1184 (2016).
3. J. A. Otkin, M. C. Anderson, C. Hain, M. Svoboda, Examining the relationship between drought development and rapid changes in the evaporative stress index. *J. Hydrometeorol.* **15**, 938–956 (2014).
4. J. A. Otkin *et al.*, Flash droughts: A review and assessment of the challenges imposed by rapid-onset droughts in the United States. *Bull. Am. Meteorol. Soc.* **99**, 911–919 (2018).
5. R. D. Koster, S. D. Schubert, H. Wang, S. P. Mahanama, A. M. Deangelis, Flash drought as captured by reanalysis data: Disentangling the contributions of precipitation deficit and excess evapotranspiration. *J. Hydrometeorol.* **20**, 1241–1258 (2019).
6. M. Osman *et al.*, Flash drought onset over the contiguous United States: Sensitivity of inventories and trends to quantitative definitions. *Hydrol. Earth Syst. Sci.* **25**, 565–581 (2021).
7. T. Parker, A. Gallant, M. Hobbins, D. Hoffmann, Flash drought in Australia and its relationship to evaporative demand. *Environ. Res. Lett.* **16**, 064033 (2021).
8. J. Lisonbee, M. Woloszyn, M. Skumanich, Making sense of flash drought: Definitions, indicators, and where we go from here. *J. Appl. Serv. Climatol.* **2021**, 1–19 (2021).
9. T. W. Ford, C. F. Labosier, Meteorological conditions associated with the onset of flash drought in the Eastern United States. *Agric. For. Meteorol.* **247**, 414–423 (2017).
10. K. C. Mo, D. Plettenmaier, Prediction of flash droughts over the United States. *J. Hydrometeorol.* **21**, 1793–1810 (2020).
11. J. A. Otkin *et al.*, Examining Rapid Onset Drought Development Using the Thermal Infrared–Based Evaporative Stress Index. *Journal of Hydrometeorology* **14**, 1057–1074 (2013).
12. M. C. Anderson *et al.*, An intercomparison of drought indicators based on thermal remote sensing and NLDAS-2 simulations with U.S. drought monitor classifications. *J. Hydrometeorol.* **14**, 1035–1056 (2013).
13. M. T. Hobbins *et al.*, The evaporative demand drought index. Part I: Linking drought evolution to variations in evaporative demand. *J. Hydrometeorol.* **17**, 1745–1761 (2016).
14. D. J. McEvoy *et al.*, The evaporative demand drought index. Part II: CONUS-wide assessment against common drought indicators. *J. Hydrometeorol.* **17**, 1763–1779 (2016).
15. A. G. Pendergrass *et al.*, Flash droughts present a new challenge for subseasonal-to-seasonal prediction. *Nat. Clim. Chang.* **10**, 191–199 (2020).
16. J. Flexas *et al.*, Steady-state chlorophyll fluorescence (Fs) measurements as a tool to follow variations of net CO2 assimilation and stomatal conductance during water-stress in C3 plants. *Physiol. Plant.* **114**, 231–240 (2002).
17. Y. Yoshida *et al.*, The 2010 Russian drought impact on satellite measurements of solar-induced chlorophyll fluorescence: Insights from modeling and comparisons with parameters derived from satellite reflectances. *Remote Sens. Environ.* **166**, 163–177 (2015).
18. L. Liu *et al.*, Evaluating the utility of solar-induced chlorophyll fluorescence for drought monitoring by comparison with NDVI derived from wheat canopy. *Sci. Total Environ.* **625**, 1208–1217 (2018).
19. F. Tian *et al.*, Exceptional drought across Southeastern Australia caused by extreme lack of precipitation and its impacts on NDVI and SIF in 2018. *Remote Sens.* **12**, 54 (2019).
20. F. Daumard *et al.*, A field platform for continuous measurement of canopy fluorescence. *IEEE Trans. Geosci. Remote Sens.* **48**, 3358–3368 (2010).
21. C. Frankenberg, A. Butz, G. C. Toon, Disentangling chlorophyll fluorescence from atmospheric scattering effects in O2 A-band spectra of reflected sun-light. *Geophys. Res. Lett.* **38**, L03801 (2011).
22. C. Frankenberg *et al.*, New global observations of the terrestrial carbon cycle from GOSAT: Patterns of plant fluorescence with gross primary productivity. *Geophys. Res. Lett.* **38**, L17706 (2011).
23. C. Frankenberg *et al.*, Prospects for chlorophyll fluorescence remote sensing from the Orbiting Carbon Observatory-2. *Remote Sens. Environ.* **147**, 1–12 (2014).
24. J. Joiner *et al.*, First observations of global and seasonal terrestrial chlorophyll fluorescence from space. *Biogeosciences* **8**, 637–651 (2011).
25. L. Guanter *et al.*, Global and time-resolved monitoring of crop photosynthesis with chlorophyll fluorescence. *Proc. Natl. Acad. Sci. U.S.A.* **111**, E1327–E1333 (2014).
26. Y. Sun *et al.*, Overview of Solar-Induced chlorophyll Fluorescence (SIF) from the Orbiting Carbon Observatory-2: Retrieval, cross-mission comparison, and global monitoring for GPP. *Remote Sens. Environ.* **209**, 808–823 (2018).
27. X. Li, J. Xiao, Mapping photosynthesis solely from solar-induced chlorophyll fluorescence: A global, fine-resolution dataset of gross primary production derived from OCO-2. *Remote Sens.* **11**, 2563 (2019).
28. Y. Sun *et al.*, Drought onset mechanisms revealed by satellite solar-induced chlorophyll fluorescence: Insights from two contrasting extreme events. *J. Geophys. Res. Biogeosci.* **120**, 2427–2440 (2015).
29. S. Chen, Y. Huang, G. Wang, Detecting drought-induced GPP spatiotemporal variabilities with sun-induced chlorophyll fluorescence during the 2009/2010 droughts in China. *Ecol. Indic.* **121**, 107092 (2021).
30. K. E. Trenberth *et al.*, Global warming and changes in drought. *Nat. Clim. Chang.* **4**, 17–22 (2014).
31. X. Yuan, L. Wang, E. F. Wood, 17. Anthropogenic intensification of southern African flash droughts as exemplified by the 2015/16 season. *Bull. Am. Meteorol. Soc.* **99**, S86–S90 (2018).
32. Y. Qing, S. Wang, B. C. Ancell, Z. L. Yang, Accelerating flash droughts induced by the joint influence of soil moisture depletion and atmospheric aridity. *Nat. Commun.* **13**, 1–10 (2022).
33. D. B. Lobell, M. Bänziger, C. Magorokosho, B. Vivek, Nonlinear heat effects on African maize as evidenced by historical yield trials. *Nat. Clim. Chang.* **1**, 42–45 (2011).
34. E. E. Butler, P. Huybers, Variations in the sensitivity of US maize yield to extreme temperatures by region and growth phase. *Environ. Res. Lett.* **10**, 034009 (2015).
35. G. Duveiller, A. Cescatti, Spatially downscaling sun-induced chlorophyll fluorescence leads to an improved temporal correlation with gross primary productivity. *Remote Sens. Environ.* **182**, 72–89 (2016).
36. G. Duveiller *et al.*, A spatially downscaled sun-induced fluorescence global product for enhanced monitoring of vegetation productivity. *Earth Syst. Sci. Data* **12**, 1101–1116 (2020).
37. C. Frankenberg *et al.*, Downscaled GOME2 SIF. [Data set]. European Commission, Joint Research Centre. (2019) https://doi.org/10.2905/21935FFC-B797-4BEE-94DA-8FEC85B3F9E1.
38. J. T. Abatzoglou, Development of gridded surface meteorological data for ecological applications and modelling. *Int. J. Climatol.* **33**, 121–131 (2013).
39. B.-T. Jong, M. Newman, A. Hoell, Subseasonal meteorological drought development over the central United States during Spring. *J. Clim.* **35**, 2525–2547 (2022).
40. R. D. Koster *et al.*, Regions of strong coupling between soil moisture and precipitation. *Science* **305**, 1138–1140 (2004).
41. G. Wang, Y. Kim, D. Wang, Quantifying the strength of soil moisture–precipitation coupling and its sensitivity to changes in surface water budget. *J. Hydrometeorol.* **8**, 551–570 (2007).
42. Y. Kim, G. Wang, Impact of vegetation feedback on the response of precipitation to antecedent soil moisture anomalies over North America. *J. Hydrometeorol.* **8**, 534–550 (2007).
43. Y. Kim, G. Wang, Soil moisture-vegetation-precipitation feedback over North America: Its sensitivity to soil moisture climatology. *J. Geophys. Res. Atmos.* **117**, 18115 (2012).
44. Q. Mu, F. A. Heinsch, M. Zhao, S. W. Running, Development of a global evapotranspiration algorithm based on MODIS and global meteorology data. *Remote Sens. Environ.* **111**, 519–536 (2007).
45. Q. Mu *et al.*, Evaluating water stress controls on primary production in biogeochemical and remote sensing based models. *J. Geophys. Res. Biogeosci.* **112**, 1012 (2007).
46. Y. Jiang, M. Yang, W. Liu, K. Mohammadi, G. Wang, Eco-hydrological responses to recent droughts in tropical South America. *Environ. Res. Lett.* **17**, 024037 (2022).
47. T. S. Magney *et al.*, Mechanistic evidence for tracking the seasonality of photosynthesis with solar-induced fluorescence. *Proc. Natl. Acad. Sci. U.S.A.* **116**, 11640–11645 (2019).
48. J. A. Otkin, M. C. Anderson, C. Hain, M. Svoboda, Using temporal changes in drought indices to generate probabilistic drought intensification forecasts. *J. Hydrometeorol.* **16**, 88–105 (2015).
49. K. Mohammadi, Y. Jiang, G. Wang, Flash drought early warning based on the trajectory of solar-induced chlorophyll fluorescence. GitHub. https://github.com/KoushanM/Flash-drought-early-warning. Deposited 20 July 2022.